Progress of Theoretical Physics, Vol. 71, No. 1, January 1984

Fractal Basin Structure

Shinji TAKESUE and Kunihiko KANEKO

Department of Physics, University of Tokyo, Tokyo 113

(Received August 1, 1983)

The basin structure of a class of one-dimensional mappings is studied. In a model proposed by the present authors, the basin of attraction is separated into uncountable pieces of open intervals and has a kind of self-similarity. Symbolic sequences are used to elucidate the structure. The way of breakdown of the structure due to a noise is studied on the basis of the analysis using symbolic sequences. The effect of noise on a crisis is discussed.

§ 1. Introduction

Revealing novel and essential aspects in nonlinear physics is one of the most important problems in our age. The recent advance in this field has thrown light on various phenomena, such as the period-doubling, intermittency and collapse of tori. There remains, however, a fundamental problem, characteristic of nonlinear phenomena. That is the analysis of basin structure in multibasin systems.[1)~11)]

More than one attractors can coexist in a lot of nonlinear systems. Typical and simple examples appear in certain one-dimensional mappings[2)~5),*)] and in two-dimensional mappings.[6)~11)] Mandelbrot[7)] has shown that the basin boundary of a certain analytic map on the complex plane is fractal, which has attracted many authors and has been investigated.[9),10)] On the other hand, one of the present authors (K. K.)[11)] has found the "self-similar basin structure" in a two-dimensional map and has related it to the stretching at the periodic saddle.

In the present paper, we focus our attention mainly on the basin structure itself, not on the basin boundary.

In §2, "fractal basin structures" are revealed by using a class of one-dimensional mappings. The structure is caused by a topological chaos[12)] present between coexisting attractors. It has infinitesimal structures and has a kind of scaling property. We analyze the structure utilizing symbolic sequences, i.e., so-called "itineraries".[13)] Each unit of the basin structure corresponds to a symbolic sequence and the characteristic features of the fractal basin structures are understood by the itineraries.

In §3, the effect of noise on the structure is analyzed. We introduce the notion of probability into the basin of attraction. The probability to go to one attractor is calculated on the basis of the itinerary analysis. The small structure is destroyed by a small noise, while the large one survives. The scaling between the size of the structure and the strength of the noise is represented by a "stability number", which is given through the above analysis. In that section we make use of some properties of linear stochatic difference equations, shown in the Appendix.

Section 4 is devoted to the critical behavior near the crisis.[14)] The effect of noise on the lifetime of the chaotic transient[15)] is calculated.

*) Multibasin can appear in a one-dimensional map on an interval with multi-humps or positive Schwarzian derivative.

Discussion and a summary are given in §5.

§ 2. Fractal basin structure

In this section we present a typical example of the one-dimensional iterated mappings which exhibit a fractal basin structure. Evidently our model must have at least two attractors. For simplicity, one of the attractors denoted by (+) is assumed to be in the region $(1, \infty)$, and the other (−) in $(-\infty, -1)$. It is also assumed that each of these semi-infinite intervals is a part of the basin of attraction of the attractor contained in it. Under these approximations it is necessary for the fractal basin structure to occur that a topological chaos and a set of points mapped into the outer regions $(1, \infty)$ and $(-\infty, -1)$ exist in the remaining interval $[-1, 1]$. One of the simplest models of such mappings in the interval is the following piecewise linear one:

$$x_{n+1}=f(x_n), \tag{2·1}$$

$$f(x)=\begin{cases} f_L(x)=-1+\beta^{-1}(x+1) & \text{for } -1\leqq x\leqq -\alpha(1-\beta)/(\alpha+\beta), \\ f_C(x)=-\alpha^{-1}x & \text{for } |x|<\alpha(1-\beta)/(\alpha+\beta), \\ f_R(x)=1+\beta^{-1}(x-1) & \text{for } \alpha(1-\beta)/(\alpha+\beta)\leqq x\leqq 1, \end{cases} \tag{2·2}$$

where $0<\alpha<1$ and $0<\beta<1/2$. For later convenience, we give here also the inverse functions of (2·2).

$$f_L^{-1}(x)=-1+\beta(x+1), \tag{2·3a}$$

$$f_C^{-1}(x)=-\alpha x\ , \tag{2·3b}$$

$$f_R^{-1}(x)=1+\beta(x-1). \tag{2·3c}$$

When $\alpha+2\beta>1$, this model has a chaotic attractor $[-(1-\beta)/(\alpha+\beta), (1-\beta)/(\alpha+\beta)]$ and its basin of attraction is the whole open interval $(-1, 1)$. As $\alpha+2\beta$ decreases, the chaotic attractor extends its domain, and at $\alpha+2\beta=1$, it touches the unstable fixed points ± 1. Such an event is called a crisis and extensively studied by Grebogi et al.[14] For $\alpha+2\beta<1$, the chaotic attractor disappears but the topological chaos remains to exist. The graph of the function $f(x)$ in this case is depicted in Fig. 1. Here, if a point comes into the region $(2\beta-1, -\alpha)$ after a number of iterates of the mapping, it escapes from the interval $[-1, 1]$ to enter the right outer region $(1, \infty)$ after one more iterate. On the other hand, once a point enters the interval $(\alpha, 1-2\beta)$, it jumps into the left outer region $(-\infty, -1)$ at the next step. Namely, the preimages of points in the "gate" $(2\beta-1, -\alpha)$ belong to the basin of attraction of the attractor (+), and the preimages of points in the other gate $(\alpha, 1-2\beta)$ belong to that of the attractor (−). These two types of points make an infinite number of open intervals which are pieces of the basins of attrac-

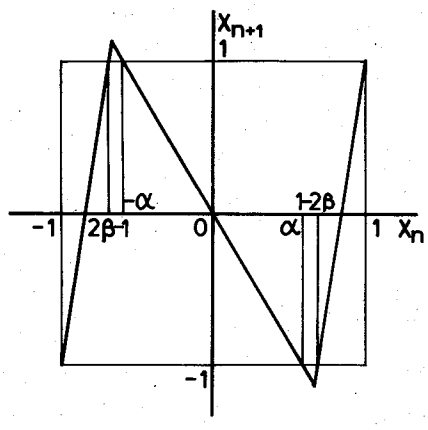

Fig. 1. The piecewise linear mapping $x_{n+1}=f(x_n)$ when $\alpha+2\beta<1$.

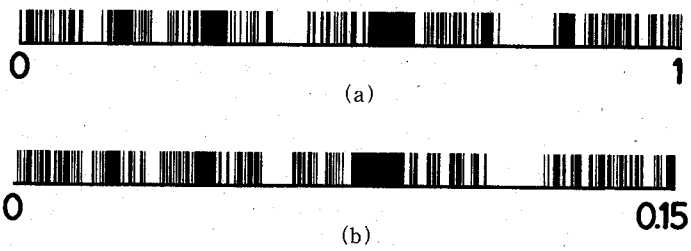

Fig. 2. The fractal basin structure exhibited by the mapping f in the intervals (a) $[0, 1]$ and (b) $[0, 0.15]$. Here the parameters are chosen to be $\alpha=8/11$ and $\beta=2/21$. Five hundred points were chosen in each interval to examine to which basin they belong. In the shaded region the orbits from the representative points hit the gate to the attractor $(+)$ $(2\beta-1, -\alpha)$. The large scale structure is identical in both figures. Though the fine structure is seen apparently different, the appearance of it depends on the representative points, because the structures smaller than the coarse graining length are present.

tion individually. Moreover, there are infinitely many such intervals between any two of them. The structure has a self-similarity, that is, if we magnify a region containing an infinite number of the pieces of the basins by an appropriate scale, the identical structure to the original one appears. This is the fractal basin structure which is the center of our interest. In fact, the boundary of the basins makes a fractal set or a Fatou dust whose dimension D is determined by the relation $\alpha^D+2\beta^D=1$.[7] An example of the fractal basin structure is shown in Fig. 2.

Now we introduce the itinerary according to the book of Collet and Eckmann as follows. The itinerary $\boldsymbol{I}(x)=I_0(x)I_1(x)\cdots$ is either an infinite sequence of symbols L's, R's and C's or a finite sequence of L's, M's and C's followed by G^+ or G^-. The jth character $I_j(x)$ or $\boldsymbol{I}(x)$ is defined by the following rule.

$$I_j(x)=\begin{cases} L & \text{if } f^j(x)\in[-1,\ 2\beta-1], \\ G^+ & \text{if } f^j(x)\in(2\beta-1,\ -\alpha), \\ C & \text{if } f^j(x)\in[-\alpha,\ \alpha], \\ G^- & \text{if } f^j(x)\in(\alpha,\ 1-2\beta), \\ R & \text{if } f^j(x)\in[1-2\beta,\ 1], \end{cases} \tag{2·4}$$

where $f^j(x)$ denotes the jth iterate of the mapping f.

We define here also some notions concerning itineraries for the later use. A symbolic sequence $\boldsymbol{I}$ is called admissible if a number $x\in[-1, 1]$ exists such that $\boldsymbol{I}(x)=\boldsymbol{I}$. Thus all of the infinite sequences of L's, R's and C's and all of the finite ones followed by G^+ or G^- are admissible in our model (2·2). The cardinality of a symbolic sequence $\boldsymbol{I}$ is denoted by $|\boldsymbol{I}|$. Furthermore, the set of points indicated by $\boldsymbol{I}$ (it is not necessary to be admissible) is represented by $\mathcal{J}(\boldsymbol{I})$, that is,

$$\mathcal{J}(\boldsymbol{I})=\{x|\ I_j(x)=I_j \quad \text{for } 0\leqq j<|\boldsymbol{I}|\}. \tag{2·5}$$

For example, $\mathcal{J}(G^+)=(2\beta-1, -\alpha)$ and $\mathcal{J}(R)=[1-2\beta, 1]$. Especially the set $\mathcal{J}(\boldsymbol{I})$ is empty unless $\boldsymbol{I}$ is either an admissible sequence or a finite one of R's, L's and C's which we call a cylinder. The measure of $\mathcal{J}(\boldsymbol{I})$ is denoted by $|\mathcal{J}(\boldsymbol{I})|$. The ordering "$<$" between different admissible sequences can be defined also in the same manner as in the case of unimodal mappings.[13] At first, we define the symbols' order that $L<G^+<C<G^-$

$<R$. Then we say $\boldsymbol{A}<\boldsymbol{B}$ for different admissible sequences $\boldsymbol{A}$ and $\boldsymbol{B}$ if either there are an even number of C in $A_0A_1\cdots A_{i-1}=B_0B_1\cdots B_{i-1}$ and $A_i<B_i$ or there are an odd number of C in $A_0A_1\cdots A_{i-1}=B_0B_1\cdots B_{i-1}$ and $B_i<A_i$. This ordering is clearly complete and leads to the following relations:

$$\textit{If } x<x', \textit{ then } \boldsymbol{I}(x)\leqq\boldsymbol{I}(x')$$

$$\textit{and if } \boldsymbol{I}(x)<\boldsymbol{I}(x'), \textit{ then } x<x'.$$

The points in the interval $[-1, 1]$ can be classified according to their itineraries. Particularly, the following two statements hold:

(i) For an admissible sequence $\boldsymbol{I}$ of an infinite length (i.e., $|\boldsymbol{I}|=\infty$), the point $x\in\mathcal{J}(\boldsymbol{I})$ is unique and the orbit initialized at x either is chaotic in the sense of Li and Yorke,[16] or eventually falls onto an unstable fixed point or cycle. Such points make a Cantor set.

(ii) For an admissible sequence $\boldsymbol{I}$ with a finite length $|\boldsymbol{I}|=m+1$, the set $\mathcal{J}(\boldsymbol{I})$ is an open interval which is a piece of the basin of attraction for the attractor $(+)$ or $(-)$ corresponding to the last character of the sequence I_m being G^+ or G^-, respectively.

In fact the statement (i) does not always hold for the models exhibiting the fractal basin structure. Some more conditions are needed for the mapping function f in (2·1), e.g., it is necessary that there is no stable point or cycle in $[-1, 1]$ and it is sufficient that f is piecewise monotone with its derivative $|df/dx|>1$ in the region such that $|f|\leqq 1$. When the latter condition holds, we can construct the sequence of closed intervals $\mathcal{J}_0$, $\mathcal{J}_1$, $\mathcal{J}_2\cdots$ defined by $\mathcal{J}_n=\mathcal{J}(I_0I_1\cdots I_n)$ for the infinite admissible sequence $\boldsymbol{I}=I_0I_1I_2\cdots$ to satisfy $|\mathcal{J}_{n+1}|/|\mathcal{J}_n|\leqq(\max|df/dx|)^{-1}<1$. Consequently this sequence converges to a point as n goes to infinity.

Now, the self-similar structure of basin is evident from that of the symbolic sequences and the statement (ii). The former means that the set of all finite admissible sequences is transformed onto itself by the shift operation, where the shift operator $\mathcal{S}$ is defined by $\mathcal{S}(I_0I_1I_2\neq)=I_1I_2\cdots$. Thus the statement (ii) indicates that the set of the pieces of basins $\{\mathcal{J}(\boldsymbol{I}): \boldsymbol{I}\in\Sigma\}$ generated by the set of finite admissible sequences Σ such that the set of all the finite admissible sequences is obtained by a number of the shift operation, contains the identical structure to the set of all the pieces of basins. In other words, the interval corresponding to a cylinder has the same basin structure as the whole interval $[-1, 1]$ except for its scale.

In fact we can construct a linear homeomorphism $f_{\boldsymbol{s}}$: $\mathcal{J}(\boldsymbol{s})\to[-1, 1]$ for the cylinder $\boldsymbol{s}$ with the length $|\boldsymbol{s}|=m$ in the following form:

$$f_{\boldsymbol{s}}=f_{s_{m-1}}\circ f_{s_{m-2}}\circ\cdots\circ f_{s_0}, \tag{2·6}$$

where $f\circ g(x)$ means $f(g(x))$. Its inverse is given by

$$f_{\boldsymbol{s}}^{-1}=f_{s_0}^{-1}\circ f_{s_1}^{-1}\circ\cdots\circ f_{s_{m-1}}^{-1}. \tag{2·7}$$

This allows us to obtain the interval $\mathcal{J}(\boldsymbol{I})$ for the finite admissible sequence $\boldsymbol{I}$ given by $I_j=s_j$ for $0\leqq j\leqq m-1$ and $I_m=G(=G^+$ or $G^-)$. It is written as

$$\mathcal{J}(\boldsymbol{I})=f_{\boldsymbol{s}}^{-1}(\mathcal{J}(G)). \tag{2·8}$$

Afterwards we also write $f_{\boldsymbol{I}}$ in place of $f_{\boldsymbol{s}}$ when the above relation exists between $\boldsymbol{I}$ and $\boldsymbol{s}$.

If a function g is linear, the nth iterate of g is easily obtained, that is,

$$\text{if } g(x)=Ax+B, \quad \text{then } g^n(x)=A^nx+\frac{1-A^n}{1-A}B\,. \tag{2·9}$$

Thus if the admissible sequence has the repeated structure of a shorter sequence, the interval for it is easily obtained. For example, if $\boldsymbol{I}=C^mG^+\equiv C\cdots CG^+$, the inverse homeomorphism (2·7) is

$$f_I^{-1}(x)=f_C^{-m}(x)=(-\alpha)^m x\,. \tag{2·10}$$

By using Eq. (2·8), we have

$$\mathcal{J}(C^mG^+)=((-\alpha)^m(2\beta-1);(-\alpha)^{m+1}). \tag{2·11}$$

The length of the interval $|\mathcal{J}(\boldsymbol{I})|$ is more easily derived. If the length of sequence $|\boldsymbol{I}|=m+1$ and the number of C's contained in I is l, it is given by

$$|\mathcal{J}(\boldsymbol{I})|=\alpha^l\beta^{m-l}(1-\alpha-2\beta). \tag{2·12}$$

This reflects the scale invariance of the fractal basin structure having two scales α and β. If we make one of the scales vanish, it appears a self-similar structure with a single scale. The graph of the mapping f in each case is shown in Figs. 3(a) and (b). Here the

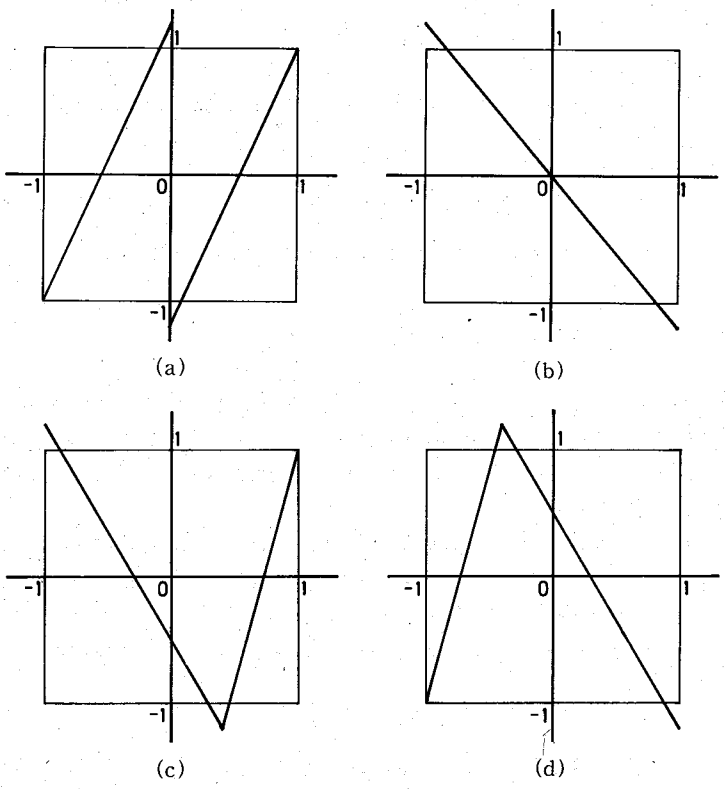

Fig. 3. The graphs of the mapping function f in the various limits: (a)$\alpha\to 0$, (b)$\beta\to 0$, (c) $\beta\to 0$ in f_L only and (d) $\beta\to 0$ in f_R only.

continuity of f is lost. In Fig. 3(a), we have shown the case $\alpha=0$, in which $\mathcal{J}(G^+)$ comes into contact with $\mathcal{J}(G^-)$. The topological chaos remains to exist in this case. Thus the fractal basin structure also survives. On the contrary, in Fig. 3(b) we have shown the case $\beta=0$, in which the topological chaos disappears. Then, the fractal basin structure also vanishes. Instead, the stripe structure of basin[11] appears. Here a self-similarity can be seen only about the origin, which results from the fact that there remains only a type of cylinder C^n. We can also consider the case that β in the left or right domain only becomes zero. The graph of f in each case is shown in Figs. 3(c) and (d) respectively. Remark also that the continuity is lost at a boundary of $[-1, 1]$. In these cases, the fractal basin structure remains to exist as in the case Fig. 3(a). Besides the scale invariance, it can also be easily shown by using (2·12) that the sum of the length of the intervals corresponding to the finite admissible sequences equals the length of the whole interval $[-1, 1]$.

Our above analysis has been based upon the piecewise linear model defined by (2·2). However, it can be applied with a little modification to models with the mapping function piecewise monotone in the region where the value of the function is in the interval $[-1, 1]$. An example is the following model:

$$f(x)=Ax^3+(1-A)x\ . \tag{2·13}$$

For $A>4$, this model shows the fractal basin structure with many scales.

§ 3. Noise effect on the fractal basin structure

In this section we study how the fractal basin structure described in the last section is destroyed by a noise added to our model. Therefore the mapping (2·1) is modified into the following stochastic process:

$$X_{n+1}=f(x_n)+\eta_n\ , \tag{3·1}$$

where the noise $\{\eta_n\}$ is assumed to be gaussian white and stationary for simplicity, that is,

$$\langle\eta_n\rangle=0\ , \qquad \langle\eta_n\eta_{n'}\rangle=\varepsilon\delta_{nn'}\ . \tag{3·2}$$

The present basin should become stochastic conceptually. Therefore, we will treat the probability $p_+(x)$ that the orbit started from the point x enters the right outer region $(1, \infty)$ when it leaves the interval $[-1, 1]$ for the first time. We evaluate this quantity approximately in the following.

If the point x lies in the open interval $\mathcal{J}(\boldsymbol{I})$ corresponding to the admissible sequence $\boldsymbol{I}$ with the cardinality $|\boldsymbol{I}|=m+1<\infty$, most of the sample paths of the stochastic process (3·1) should trace such trajectories that $f^j(x)\in\mathcal{J}(I_j)$ for $j\leqq m$ in the case of small ε. If it is the case, we may replace Eq. (3·1) by the following linear stochastic process:

$$X_{n+1}=f_{I_n}(X_n)+\eta_n \tag{3·3}$$

within a fairly good approximation. Here the domains of the functions f_{I_n} are extended to the entire real number $(-\infty, \infty)$. This type of equations will be discussed in the Appendix and the results obtained there are used here. Namely, for the initial distribu-

tion $P_0(X)=\delta(X-x)$, the distribution after the nth iterate of the mapping (3·3) is given by

$$P_n(X)=\frac{1}{\sqrt{2\pi\sigma_n}}\exp\left\{-\frac{(X-x_n)^2}{2\sigma_n}\right\}, \tag{3·4}$$

where the parameters are defined by

$$x_n=f_{I_{n-1}}\circ f_{I_{n-2}}\circ\cdots\circ f_{I_0}(x), \tag{3·5}$$

$$\begin{aligned}\sigma_n&=\varepsilon g_{I_{n-1}}\circ g_{I_{n-2}}\circ\cdots\circ g_{I_0}(0)\\&=\varepsilon g_{I_{n-1}}\circ g_{I_{n-2}}\circ\cdots\circ g_{I_0}(1),\end{aligned} \tag{3·6}$$

together with the functions g defined by

$$\begin{aligned}g_C(\sigma)&=\alpha^{-2}\sigma+1,\\g_R(\sigma)&=g_L(\sigma)=\beta^{-2}\sigma+1.\end{aligned} \tag{3·7}$$

Our next approximation is that the sample paths entering $\mathcal{J}(I_m)$ after the mth iterate should go to the same attractor as in the noiseless case and that other sample paths are expected to go to each attractor with probability 1/2. Under these approximations, the probability $p_+(x)$ can be written as

$$p_+(x)=\frac{1}{2}\left\{1\pm\int_{\mathcal{J}(I_m)}P_m(X)dX\right\}, \tag{3·8}$$

where the sign $\pm$ corresponds to that of the symbol $I_m=G^+$ or G^-.

Since the distribution $P_m(X)$ is gaussian having the center at $X=x_m$ in the interval $\mathcal{J}(I_m)$ and the variance σ_m, the integral on the right-hand side of (3·8) gives almost unity if the distance between x_m and the nearby endpoint of $\mathcal{J}(I_m)$ is much greater than the standard deviation $\sqrt{\sigma_m}$. As $\sqrt{\sigma_m}$ is increased, the value of the integral gradually decreases and changes largely when the two quantities become comparable. Finally the integral becomes nearly zero for $\sqrt{\sigma_m}$ much larger than the distance. Our approximate result (3·8) becomes wrong in the latter case, because then the effect of the paths that escape from the interval $[-1, 1]$ before arriving at $\mathcal{J}(I_m)$ cannot be neglected. Thus, in that case, the integral in (3·8) is replaced by

$$\sum_{l=1}^{m}\left\{\int_{\mathcal{J}(G^+)}P_l(X)dX-\int_{\mathcal{J}(G^-)}P_l(X)dX\right\}. \tag{3·9}$$

Here, we have neglected the influence of escapes upon the later distribution, because it is expected to be small.

Figure 4 shows the change of the value of $p_+(x)$ as a function of the strength of noise $\sqrt{\varepsilon}$. As is shown in this figure, it is possible that a point originally in a basin of attraction of one attractor is apt to prefer going to the other due to the noise. It is nothing but the reflection of a nearby large structure, which is comprehended through (3·9).

When the integral in (3·8) becomes negligible even for the center of the interval $\mathcal{J}(\boldsymbol{I})$, the structure of $\boldsymbol{I}$ cannot be seen in the function $p_+(x)$. The condition for it is expressed as

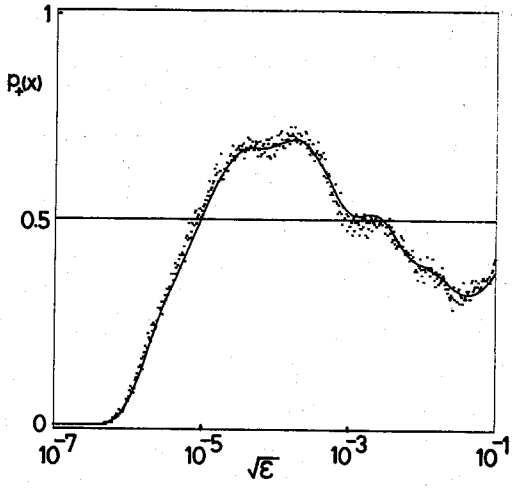

Fig. 4. The probability $p_+(x)$ for $x=-0.592509$ as a function of $\sqrt{\varepsilon}$. Dots represent the results of the numerical simulation in which a thousand trials per point were executed. The solid line was obtained from (3·9).

$$\sqrt{\sigma_m} \gg \frac{1}{2}|\mathcal{J}(I_m)| = \frac{1-\alpha-2\beta}{2}. \qquad (3\cdot10)$$

By using (3·7) and setting $\bar{\sigma}_I = g_{I_{m-1}} \circ g_{I_{m-2}} \circ \cdots \circ g_{I_0}(0)$, it is rewritten into the following form:

$$\sqrt{\varepsilon} \gg \frac{1-\alpha-2\beta}{\sqrt{\bar{\sigma}_I}}. \qquad (3\cdot11)$$

The right-hand side of the above inequality in expressed only by the nature of $\boldsymbol{I}$. Therefore, it represents the stability of the structure $\boldsymbol{I}$ against the noise. The meaning of it is as follows. If the standard deviation of noise $\sqrt{\varepsilon}$ is much less than this stability number, the structure of $\boldsymbol{I}$ is essentially the same as in the noiseless case, that is, it is decided almost deterministically to which attractor the points in the interval $\mathcal{J}(\boldsymbol{I})$ should go. If $\sqrt{\varepsilon}$ is of the same degree as the stability of $\boldsymbol{I}$, the structure $\boldsymbol{I}$ remains to exist but becomes stochastic. On the other hand, when the condition (3·11) is satisfied, the structure of $\boldsymbol{I}$ is destructed and $p_+(x)$ varies slowly and in the interval $\mathcal{J}(\boldsymbol{I})$.

The stability number is independent of the first character of the symbolic sequence because $g_{I_0}(0)$ is always unity. Thus for example, the structures $CRCLG^+$ and $RRCLG^+$ have the same stability. It is also independent of the last character G^+ or G^- owing to the symmetry in our piecewise linear model. Between sequences with a common first character, the stability numbers are approximately in proportion to the length of intervals indicated by the sequences. In fact, the stability becomes exactly proportional to the length of the interval, if the constant terms on the right-hand sides of (3·7) are omitted.

We have carried out the numerical simulation in order to see the behavior above described. Figures 5 show how the fractal basin structure in the interval $[-0.7085, -0.6985]$ is destructed as the strength of noise ε is changed. Here the parameters are chosen to be $\alpha=8/11$ and $\beta=2/21$, at which this interval contains $\mathcal{J}(CRCL)=[-0.7083825266\cdots, -0.698787504\cdots]$. The most stable structures in it are $CRCLG^+$ and $CRCLG^-$, and their stability number is $2.6942\cdots\times10^{-4}$. The standard deviations of the noise $\sqrt{\varepsilon}$ are 5×10^{-5}, 1×10^{-4}, 2×10^{-4}, 4×10^{-4} and 8×10^{-4} respectively. We have chosen five hundred points equally separated in the interval and have executed a thousand trials a point. The ratio of the trials in which the trajectories have gone to the right outer regions $(1, \infty)$ is shown in these figures.

As α is relatively large, the series of the structures $CRCLC^nG(n=0, 1, 2, \cdots)$ is dominated in $\mathcal{J}(CRCL)$. In Fig. 5(a) the series is observed up to $n=9$ and some other structures are also seen between them. In Fig. 5(b), however, every other structure has almost vanished, Though the series keeps existing up to $n=7$. Figures 5(a)~(e) show that the number of the observed structures in the series decreases by about two as the standard deviation of noise is doubled. This is consistent with our analytical results, because the stability defined in (3·11) is roughly halved by the increase of n by two.

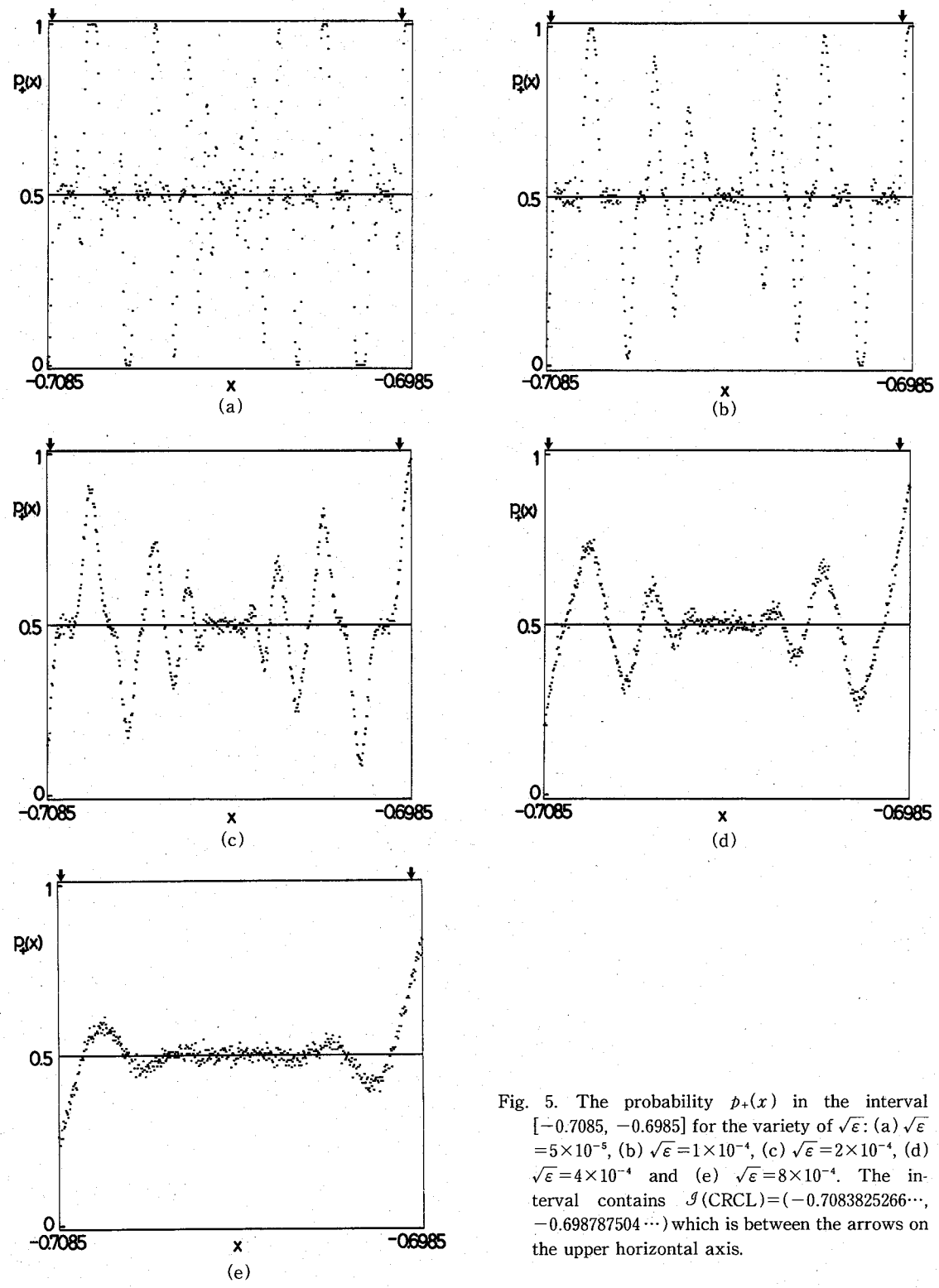

Fig. 5. The probability $p_+(x)$ in the interval $[-0.7085, -0.6985]$ for the variety of $\sqrt{\varepsilon}$: (a) $\sqrt{\varepsilon}=5\times10^{-5}$, (b) $\sqrt{\varepsilon}=1\times10^{-4}$, (c) $\sqrt{\varepsilon}=2\times10^{-4}$, (d) $\sqrt{\varepsilon}=4\times10^{-4}$ and (e) $\sqrt{\varepsilon}=8\times10^{-4}$. The interval contains $\mathcal{J}(\mathrm{CRCL})=(-0.7083825266\cdots, -0.698787504\cdots)$ which is between the arrows on the upper horizontal axis.

These figures also show that the height of the top (or the depth of the bottom) in a structure decreases and the width of it is widened to absorb the nearby fine structures with

the increase of $\sqrt{\varepsilon}$.

The self-similar structure of $p_+(x)$ is evident from Figs. 6(a) and (b). These are the magnified pictures of Fig. 5(a) around the center of the interval. These figures are very analogous to those in the original scale and having larger $\sqrt{\varepsilon}$. In fact, every interval corresponding to a cylinder has this kind of similarity, that is, $p_+(x)$'s for given two such intervals show similar graphs if the ratios of $\sqrt{\varepsilon}$ to the stability of the most stable structure in each interval are the same. This has been ascertained by the numerical simulation.

The same kind of similarity is also observed in the escape time n^* from the interval $[-1, 1]$. Figures 7(a) and (b) show the behavior of n^* as a function of initial value.

In general models other than the piecewise linear ones, the stability of a structure is hardly written down. However, it is still independent of the first character of sequence and should be approximately proportional to the width of the interval.

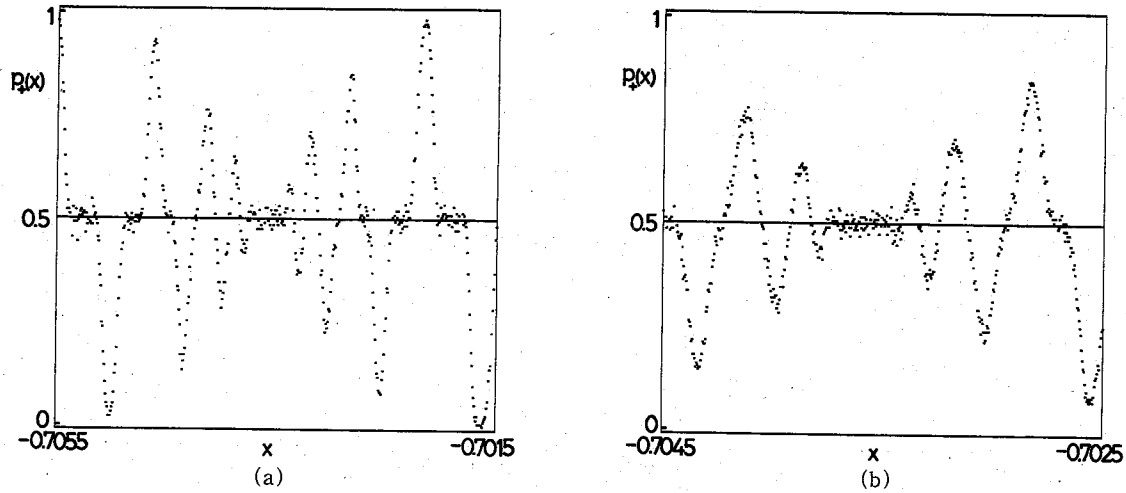

Fig. 6. Enlargements of the intervals (a) $[-0.7055, -0.7015]$ and (b) $[-0.7045, -0.7025]$ in Fig. 5(a).

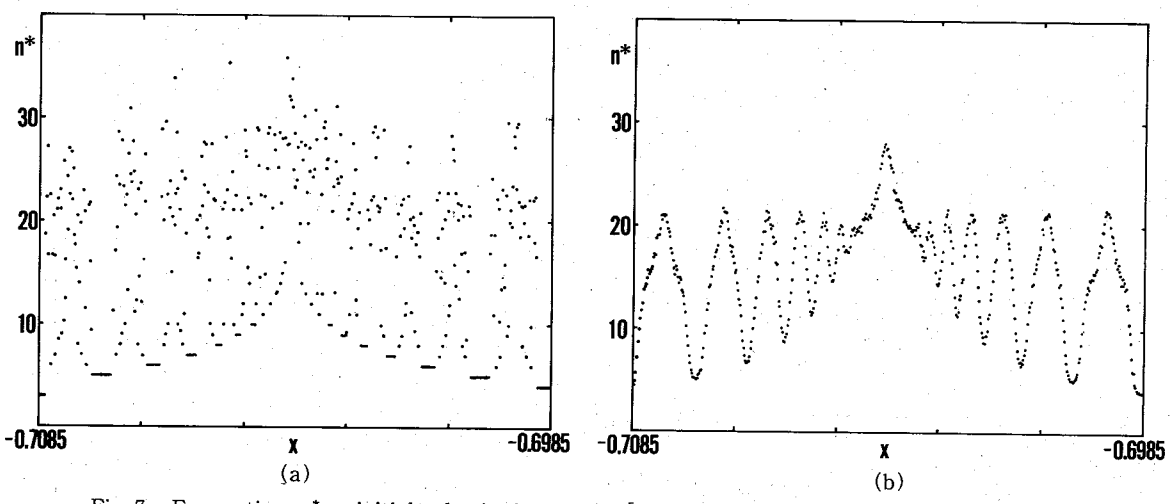

Fig. 7. Escape time n^* vs initial value in the interval $[-0.7085, -0.6985]$ for the noise amplitudes (a) $\sqrt{\varepsilon}=10^{-6}$ and (b) $\sqrt{\varepsilon}=10^{-4}$.

§ 4. Noise effect on the transition

In this section we discuss the effect of noise near a crisis in a general one-dimensional mapping, because this type of transition from chaos to transient chaos can be accompanied by the appearance of the fractal basin structure.

For simplicity we restrict our problem to the case that a chaotic attractor exists in a region and that its basin of attraction is separated by an unstable fixed point. When the chaotic attractor collides with the unstable fixed point, the transition to a transient chaos occurs. Moreover, the noise is assumed to be stationary, gaussian and white. Thus, the stochastic process treated in this section is represented by (3·1) (where $f(x)$ is general) and the probability density ρ of the noise η is given by

$$\rho(\eta)=\frac{1}{\sqrt{2\pi\varepsilon}}\exp\left(-\frac{\eta^2}{2\varepsilon}\right). \tag{4·1}$$

In the following, the mean escape rate from the chaotic region (i.e., the basin of the chaotic attractor) is asymptotically estimated for small ε when the bifurcation parameter is on the chaos side.

Without loss of generality, we can put the unstable fixed point at the origin and the chaotic region to be the negative part of the real number. The distance between the origin and the zth order maximum of f at $X=x^*$ in the chaotic region is denoted by h. Thus, the function f is approximated by

$$f(X)\simeq -h-a|X-x^*|^z \tag{4·2}$$

near $X=x^*$. Because of the mixing property of f in the chaotic region, the quasi-stationary distribution which is almost the same as the invariant measure $P(x)$ in the noiseless case is realized in a few iterations. Then the mean escape rate r is given by

$$r=\int_0^\infty dy\int dx\ P(x)\rho(y-f(x)). \tag{4·3}$$

If $P(x)$ is slowly varying near x^*, (4·3) is evaluated as

$$r\simeq\frac{P(x^*)}{\sqrt{\pi}}\int dx\ \mathrm{Erfc}\left(\frac{h+a|x-x^*|^z}{\sqrt{2\varepsilon}}\right) \tag{4·4}$$

by using Eqs. (4·1) and (4·2), where $\mathrm{Erfc}(x)=\int_x^\infty e^{-t^2}dt$. The integral in (4·4) is evaluated for the following two cases (i) $h\gg\sqrt{2\varepsilon}$ and (ii) $h\ll\sqrt{2\varepsilon}$. Then we have

$$r\simeq z\sqrt{\frac{2\varepsilon}{\pi h^2}}P(x^*)\Gamma\left(\frac{1}{z}\right)\left(\frac{\varepsilon}{ha}\right)^{1/z}e^{-h^2/2\varepsilon} \qquad \text{for Case (i)}, \tag{4·5a}$$

$$\simeq\frac{P(x^*)}{\sqrt{\pi}}\left(\frac{\sqrt{2\varepsilon}}{a}\right)^{1/z}\Gamma\left(\frac{1}{2z}+\frac{1}{2}\right) \qquad \text{for Case (ii)}. \tag{4·5b}$$

Thus we have obtained the ε-dependence of r (i) $r\propto\varepsilon^{1/2+1/z}e^{-h^2/2\varepsilon}$ and (ii) $r\propto\varepsilon^{1/2z}$, respectively.

If there are more than one points at which $f(x)$ touches the unstable fixed point, r is obtained by adding the results by (4·5) at respective points. However, when the points have some correlations, the invariant measure cannot be used for $P(x)$ and the effect of

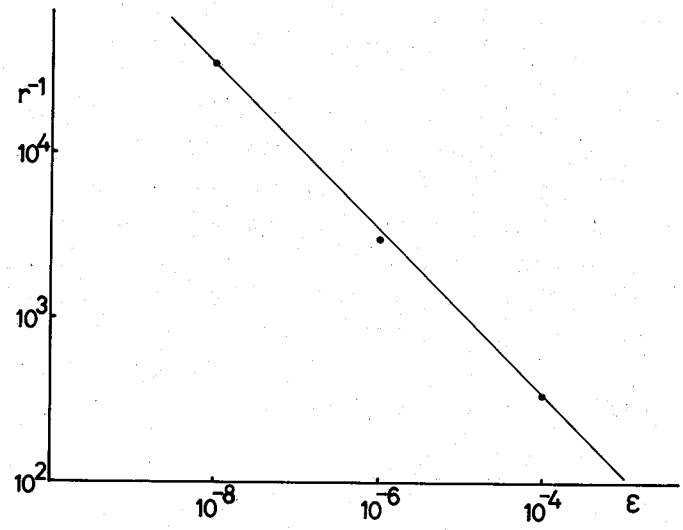

Fig. 8. The mean escape time from $[-1, 1]$ vs strength of the gaussian noise $\sqrt{\varepsilon}$. The parameters in f are $\alpha=1/10$ and $\beta=9/20$. As the distribution of the escape time is Poissonian, the mean escape time is written as r^{-1} by using the mean escape rate r. The dots represent the results of the simulation. The solid line follows from (4·6). They agree very well with each other.

the correlation should be taken into account. This applies to our piecewise linear model (2·2). When $\alpha+2\beta=1$, $f(x)$ touches the unstable fixed points ± 1 at $x=\pm 1$ and $x=\alpha$. As $f(\pm\alpha)=\mp 1$, the invariant measure $P(x)$ cannot be used for $x=\pm 1$. In this case, we transform $P(x)$ by using the Perron-Frobenius operator and substitute the result into (4·3) in place of $P(x)$. Thus we obtain

$$r\simeq\sqrt{\frac{\varepsilon}{8\pi}}\{3-\beta-(1+\beta^2)^{1/2}\}. \tag{4·6}$$

Equations (4·5) and (4·6) agree well with our numerical simulation. See Fig. 8.

§ 5. Discussion

In this paper we have investigated the fractal basin structure, which appears in a simple one-dimensional mapping. When this structure appears, the notion of basin boundary has to be changed. The boundary consists of the points in a Cantor set. The Cantor set reflects on the topological chaos. Thus, we can detect the topological chaos, which itself is not observable, through the fractal basin structure.

The complicated behavior of basin has already been noticed in Ref. 11) as a self-similar stripe structure. In that case, the boundary is not Cantor-like. Thus, the fractal basin structure is a more complex notion than the stripe structure. The one-dimensional version of the stripe structure is realized only if $\beta=0$ in the model (2·1).

The model we investigate in the present paper is mainly a piecewise-linear map with two gradients α^{-1} and β^{-1}. The fractal basin structure, however, is a rather general property which appears in a system with more than one basins separated by transient chaos. It may also appear in a noninvertible circle map if two stable cycles coexist. In

the general case, a fractal basin structure is charcterized by infinite number of scales in contrast to two scales (α and β) in the model (2·1). In this case, however, our symbolic approach is still valid and the essential feature of the structure can be understood through the present theory.

In a system with differential equations or a higher dimensional mapping, fractal basin structure is also expected. If the number of the direction of the stretching is only one, its basin structure will be explained by the present theory. If the number exceeds one, its basin structure can become more complicated, though the analysis of it will be left to the future.

In §3, we have studied the effect of noise. In experiments, the noise is inevitable. It will be of importance to perform the experiments by changing the initial condition of the system and to measure the probability that the state is attracted to one attractor, if the system has more than one attractors. Our results in §3 predict that

i) the probability $p_+(x)$ as a function of initial condition x has a self-similar structure with many scales, up to some magnitude, which is determined by the strength of noise (see Figs. 5 and 6), and

ii) if the strength of noise can be controled, the probability p_+ for some initial condition shows an oscillatory decay towards $p_+=1/2$ as the strength is increased (see Fig. 4).

In §4, the mean lifetime of the transient chaos near the crisis is calculated in the presence of noise. Depending on the ratio of the strength of noise against the distance from the critical point, two types of behavior and the crossover are obtained for the expression of the mean lifetime. It will be of importance to check these results experimentally.

Acknowledgements

The authors would like to thank Professor M. Suzuki for critical reading of the manuscript. They would also like to thank LICEPP for the facilities of FACOM M190. This study was partially financed by the Scientific Research Fund of the Ministry of Education, Science and Culture.

Appendix

—— Linear Mapping with Gaussian White Noise ——

We consider the following discrete time linear stochastic process:

$$X_{n+1}=f_n(X_n)+\eta_n\,, \tag{A·1}$$

where

$$f_n(X)=\gamma_n X+\delta_n\,, \tag{A·2}$$

and the noise $\{\eta_n\}$ is assumed to be gaussian white but non-stationary, that is,

$$\langle\eta_n\rangle=0\,,\qquad \langle\eta_n\eta_{n'}\rangle=\varepsilon_n\delta_{nn'}\,, \tag{A·3}$$

In other words, the probability density at $\eta_n=\eta$ denoted by $\rho_n(\eta)$ is given by

$$\rho_n(\eta)=\frac{1}{\sqrt{2\pi\varepsilon_n}}\exp\left(-\frac{\eta^2}{2\varepsilon_n}\right). \tag{A·4}$$

Then we can rewrite the Langevin type equation (A·1) into the Fokker-Planck type equation. Writing the probability density at $X_n=X$ as $P_n(X)$, we have

$$P_{n+1}(X)=\int dx\rho(X-f_n(x))P_n(x)$$

$$=\frac{1}{\sqrt{2\pi\varepsilon_n}}\int dxP_n(x)\exp\left\{-\frac{(X-\gamma_n x-\delta_n)^2}{2\varepsilon_n}\right\}. \tag{A·5}$$

As the equation (A·1) is linear, a gaussian distribution is mapped into another gaussian by this stochastic process. Even if an initial distribution is not gaussian, it is always represented by a sum or an integral of gaussian. Thus we may put

$$P_n(X)=\frac{1}{\sqrt{2\pi\sigma_n}}\exp\left\{-\frac{(X-x_n)^2}{2\sigma_n}\right\}. \tag{A·6}$$

Substituting this form into Eq. (A·5), we obtain

$$P_{n+1}(X)=\frac{1}{\sqrt{2\pi(\varepsilon_n+\sigma_n\gamma_n{}^2)}}\exp\left\{-\frac{(X-f_n(x_n))^2}{2(\varepsilon_n+\sigma_n\gamma_n{}^2)}\right\}. \tag{A·7}$$

This leads to the following mappings of the parameters x_n and σ_n,

$$x_{n+1}=f_n(x_n), \tag{A·8}$$

$$\sigma_{n+1}=\sigma_n\gamma_n{}^2+\varepsilon_n\equiv g_n(\sigma_n). \tag{A·9}$$

Consequently if the initial distribution $P_0(X)=\delta(X-x_0)$, the distribution after the nth iterate $P_n(X)$ is given by (A·6) and its parameters are written as

$$x_n=f_{n-1}\circ f_{n-2}\circ\cdots\circ f_0(x_0), \tag{A·10}$$

$$\sigma_n=g_{n-1}\circ g_{n-2}\circ\cdots\circ g_0(0)$$

$$=g_{n+2}\circ g_{n-2}\circ\cdots\circ g_1(\varepsilon_0). \tag{A·11}$$

Especially when the model is stationary, i.e., $\gamma_n=\gamma$, $\delta_n=\delta$ and $\varepsilon_n=\varepsilon$, we have

$$x_n=\frac{1-\gamma^n}{1-\gamma}\delta+\gamma^n x_0, \tag{A·12}$$

$$\sigma_n=\frac{1-\gamma^{2n}}{1-\gamma^2}\varepsilon. \tag{A·13}$$

References

1) K. Tomita and H. Daido, Phys. Lett. **79A** (1980), 133.
2) C. Tresser, P. Coullet and A. Arneodo, J. de Phys. Lett. **41** (1980), L243.
3) S. Fraser and R. Kapral, Phys. Rev. Lett. **A25** (1982), 3223.
4) L. Glass and R. Perez, Phys. Rev. Lett. **48** (1982), 1772.
5) K. Kaneko, Prog. Theor. Phys. **69** (1983), 403.
6) H. Daido, Prog. Theor. Phys. **63** (1980), 1190.
7) B. B. Mandelbrot, *Fractal Geometry of Nature* (Freeman, San Francisco, 1982).
8) C. Grebogi, E. Ott and J. A. Yorke, Phys. Rev. Lett. **50** (1983), 935.
9) N. S. Manton and M. Nauenberg, Commun. Math. Phys. **89** (1983), 555.
10) M. Widom, preprint.
M. Widom, D. Bensimon, L. P. Kadanoff and S. J. Shenker, preprint.
11) K. Kaneko, Prog. Theor. Phys. **69** (1983), 1427.

12) Y. Takahashi, to appear in Publ. RIMS Kyoto Univ.
13) See, for example, P. Collet and J. -P. Eckmann, *Iterated Maps on the Interval as Dynamical Systems* (Birkhäuser, 1980).
14) C. Grebogi, E. Ott and J. A. Yorke, Phys. Rev. Lett. **48** (1982), 1507.
15) J. L. Kaplan and J. A. Yorke, Commun. Math. Phys. **67** (1979), 93.
J. A. Yorke and E. D. Yorke, J. Stat. Phys. **21** (1979), 263.
16) T. Li and J. Yorke, Am. Math. Month. **82** (1975), 985.